Measurement 131 (2019) 647–653

Contents lists available at ScienceDirect

Measurement

journal homepage: www.elsevier.com/locate/measurement

Enlargement of measuring zone in laser gauges without sacrificing measurement accuracy

Yury A. Chursin *, Ludmila A. Redko, Evgeny M. Fedorov

National Research Tomsk Polytechnic University, 30, Lenin Ave., 634050 Tomsk, Russia

ARTICLE INFO

Article history:
Received 2 July 2018
Received in revised form 30 August 2018
Accepted 10 September 2018
Available online 12 September 2018

Keywords:
In-process diameter measurement
Powell lens
Optimization
Calibration

ABSTRACT

The paper proposes methods of enlarging the measuring zone in laser diameter gauges without sacrificing the measurement accuracy. Possessing a large measuring zone, such gauges are designed to measure external diameters of round wire materials whose diameter exceeds the laser diode wavelength (~0.5 mm and longer). A method of the video quality improvement is proposed herein, and algorithms are developed to detect the optimal geometrical parameters and estimate observational errors within the measuring zone of the laser diameter gauge.

1. Introduction

In existing research and industrial applications, different methods are widely used in measuring the outer diameter of products of various function and purpose. In particular, mechanical [1], magnetic [2], and ultrasonic techniques [3,4] are very common in diameter measurements. An optoelectronic technique for diameter characterization which is based on the diffraction theory in combination with image processing techniques is often used in engineering and production technology. For example, laser diameter gauges are widely used in the cable industry, which provide the distribution of both divergent and parallel beams of light [5–7]. The diameter measurement must ensure the required quality of cable products as well as the material saving and power consumption. The cable production process is complicated (Fig. 1) and requires monitoring a multitude of parameters such as eccentricity [8], unit-length capacitance [9,10], and also insulation strength testing [11,12]. The diameter gauging is performed at high speeds achieving 3000 m/min, and also at strong cable vibrations which have an adverse effect on the quality of measurements. In order to meet constantly growing demands to the measurement accuracy of cable diameters, manufacturers are forced to look for alternative techniques for reducing measuring errors.

In present-day productions, laser optoelectronic diameter gauges with a 15–60 mm measuring zone are widely used for the characterization of diameters of round wire materials [13–16]. For objective reasons, all measuring devices possess errors. During the lot production of laser diameter gauges, their adjustment and calibration take a good deal of time, but are necessitated partly by the difficulty in maintaining their all design sizes. Therefore, a manual calibration of each diameter gauge becomes impossible. For operational instruments of interest, it is very important to ensure the subscribed error throughout the entire measuring zone and not only in the vicinity of its centre, as is the case with most manufacturers. In the cable production, it's not possible to use the efficient centering methods, in particular, at a stage of wire extrusion or varnishing, when the coating is not yet polymerized. Additionally, a steady-state vibration of the product does not allow it to locate in the centre of the measuring zone. In this work we propose a range of design and algorithmic decisions allowing to create the instrument the error of which does not change when the position of the monitored object changes. We also propose a method to simplify and automate the adjustment of laser gauges in the lot production. We offer the procedures to minimize observational errors when measuring diameters with reference wire gauges. These procedures include the quality improvement of the optoelectronic diameter gauges, determination of their geometrical parameters, and automated calibration using reference gauges.

2. Material and methods

2.1. Video quality improvement

Let us consider the optical method to get the diameter value. The laser diameter gauge receives cell numbers as input parame-

* Corresponding author.
E-mail address: Ju_@tpu.ru (Y.A. Chursin).

https://doi.org/10.1016/j.measurement.2018.09.031
0263-2241/

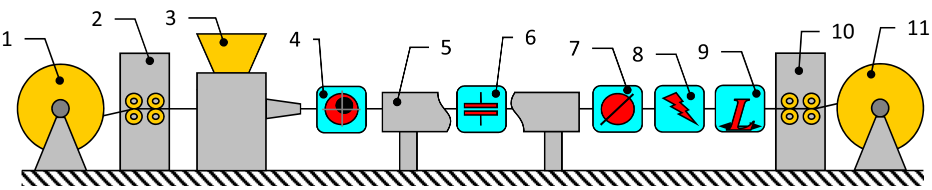

Fig. 1. Flow chart of cable production process: 1 – pay-off drum; 2 – pull-off device; 3 – extruder; 4 – eccentricity gauge; 5 – quenching bath; 6 – capacitometer; 7 – diameter gauge; 8 – high voltage tester; 9 – length and velocity measuring system; 10 – wire forming device; 11 – take-up drum.

ters which correspond to the shadow boundaries on both modules of the charge-coupled device (CCD). The detection of cells matching the shadow boundaries was presented in [17]. This geometrical model includes the point radiation sources which usually represent a semiconductor laser or a laser diode with 808 nm wavelength, the beam divergence at angles in the range of 35–42 degrees, and the power consumption ranging between 200 and 500 mW. A detailed description of the similar measuring systems was given in our previous works [18,19].

Using laser diodes without accessory optics as presented in Fig. 2 provides a range of advantages such as simplicity in design, compactness of the radiation source and its low cost. However, there are certain limitations related to the non-uniform distribution of the luminous flux within the measuring zone and its heavy losses without optimization of the laser beam. More powerful radiation sources should be used owing to the low laser beam efficiency which also increases the exposure time and causes stray light in the optical system which modifies the total observational error. Non-uniform stray lighting can lead to the additional inadmissible error. When measuring the eccentricity of a workpiece, the observational error of its position within the measuring zone should not exceed several microns. Therefore, the uniform distribution of the luminous flux should be provided within the measuring zone. As can be seen from Fig. 2, the laser diode generates a cone-shaped beam, the base of which is an ellipse having long and short axes $\theta\perp$ and $\theta//$, respectively. In this optical transducer, the orientation of laser diode allows the linear CCD to arrange along $\theta\perp$ axis and normal to $\theta//$ axis.

The luminous flux generated in $\theta\perp$ plane by an ordinary laser diode, as shown in Fig. 3, is described by the normal (or Gaussian) distribution. So, the laser intensity in the CCD centre is always higher than at its periphery. The difference between laser intensities is not problematic because the angle α limited by the length of the linear CCD module does not exceed 15–20 degrees. Local random changes in the laser intensity contribute much more to observational errors. These changes are caused by the random distribution of the luminous flux along $\theta//$ axis. Even a small difference between the relative orientation of the laser diode and CCD module leads to a non-uniform distribution of the luminous flux. Each laser diode possesses its individual properties which can cause the non-uniform distribution of the luminous flux. Additionally, the optic's surface is inevitably contaminated with dust particles or the like during the operation, thereby intensifying non-uniformity. Sometimes, it entails such troubles as the increase in observational errors and equipment failures.

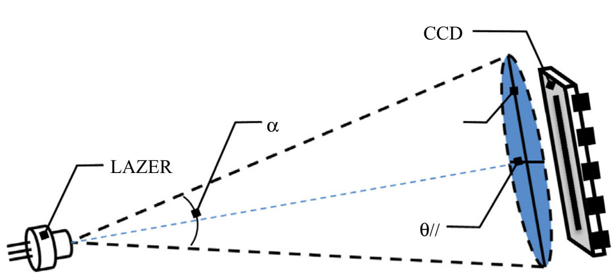

Fig. 2. Schematic orientation of laser diode without accessory optics relative to CCD module.

One of the ways to eliminate the non-uniform distribution of the luminous flux produced by the laser diode is to use the accessory optics comprising a collimator with the Powell lens. The schematic orientation of the laser diode with accessory optics is shown in Fig. 4. This method is widely used in science and technology [20–23]. The collimator is intended to obtain collimated or parallel laser beams with the diameter of 1.5–2 mm. The collimated beam transforms to the divergent beam again when passing through the Powell lens. The angle α of the beam divergence is the same, and the laser intensity distribution is uniform, without local changes. The width of the laser beam passing through the Powell lens is 1.5–2 mm. Thus, almost the whole luminous flux hits the linear CCD that allows us to apply a lower laser power and reduce the exposition time, thereby enhancing the dynamic properties of the optical system.

2.2. Optimization algorithm for geometrical parameters

The diameter of round wire materials is measured according to the proposed geometrical model presented in Fig. 5.

The optimization algorithm can be described by mathematical calculations to find the workpiece diameter. The obtained values of the shadow boundaries are transformed to physical values. Using the initial geometrical parameters, the workpiece diameter can be obtained. Let us introduce the following notation for the initial geometrical parameters:

C_x, C_y are distances respectively from the zero point to N_X and N_Y cells, where the laser beam is normal to the CCD module;
N_x, N_y are cell numbers at the points of intersection with optical axes;
H_x, H_y are distances between the CCD modules and point radiation sources.

The coordinate axes coincide with the CCD modules. At first, the cell numbers obtained for the shadow boundaries are converted into length units using the following formulas:

$$X_{11} = (N_{x1} - N_x)\mathrm{res} + C_x;$$

$$X_{21} = (N_{x2} - N_x)\mathrm{res} + C_x;$$

$$Y_{11} = (N_{y1} - N_y)\mathrm{res} + C_y;$$

$$Y_{21} = (N_{y2} - N_y)\mathrm{res} + C_y,$$

where *res* is the resolution of the CCD module, μm per cell.

Secondly, let us calculate the projection of the workpiece centre X_{01} and detect the angles of α_{x1} and β_{x1}. Next, the following equations are obtained for X_{01} and Y_{01}:

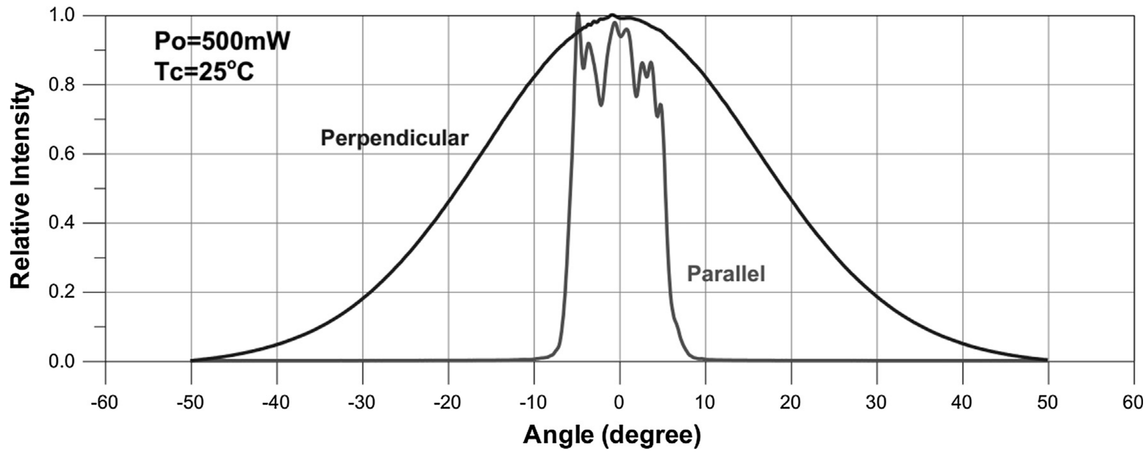

Fig. 3. Distribution of laser intensity in mutually perpendicular planes θ⊥ and θ//.

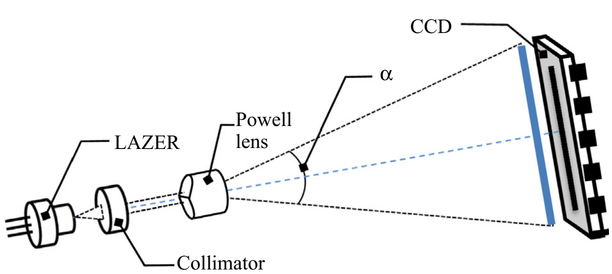

Fig. 4. Schematic orientation of laser diode with accessory optics relative to CCD module.

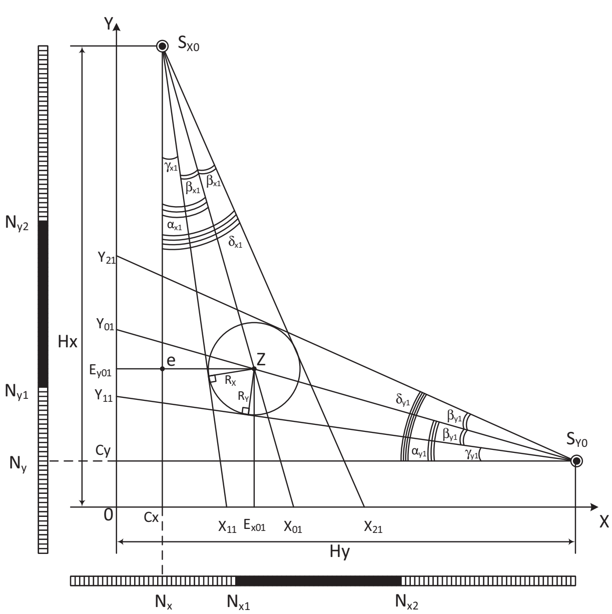

Fig. 5. Geometrical model for diameter measurement.

$$X_{01} = H_X \cdot \tan\left(\frac{1}{2}\left(\operatorname{atan}\left(\frac{X_{21} - C_X}{H_X}\right) + \operatorname{atan}\left(\frac{X_{11} - C_X}{H_X}\right)\right)\right) + C_X$$

$$Y_{01} = H_Y \cdot \tan\left(\frac{1}{2}\left(\operatorname{atan}\left(\frac{Y_{21} - C_Y}{H_Y}\right) + \operatorname{atan}\left(\frac{Y_{11} - C_Y}{H_Y}\right)\right)\right) + C_Y$$

The coordinates of the workpiece centre are determined by the system of equations derived from the similarity of triangles (S_{X0}; e; Z) and (S_{X0}; C_X; X_{01}) and those similar to the vertex S_{Y0}:

$$\begin{cases} \frac{E_{X_{01}} - C_X}{X_{01} - C_X} = \frac{H_X - E_{Y_{01}}}{H_X} \\ \frac{E_{Y_{01}} - C_Y}{Y_{01} - C_Y} = \frac{H_Y - E_{X_{01}}}{H_Y} \end{cases}$$

The solution of this system of equations allows us to obtain the coordinates of the workpiece centre:

$$E_{X_{01}} = \frac{H_y \cdot (C_X \cdot Y_{01} + H_X \cdot X_{01} - X_{01} \cdot Y_{01})}{(H_X \cdot H_Y - C_X \cdot C_Y - X_{01} \cdot Y_{01} + C_Y \cdot X_{01} + C_X \cdot Y_{01})}$$

$$E_{Y_{01}} = \frac{H_x \cdot (C_Y \cdot X_{01} + H_Y \cdot Y_{01} - X_{01} \cdot Y_{01})}{(H_X \cdot H_Y - C_X \cdot C_Y - X_{01} \cdot Y_{01} + C_Y \cdot X_{01} + C_X \cdot Y_{01})}$$

Since the workpiece is not always round, its radius should be measured both along X and Y-axes. As a result, the average diameter is determined by the laser gauge. The radius is determined by the interval between the point radiation source and the workpiece centre and the sine of the angle between this interval and the tangent to the workpiece:

$$R_{X_1} = \sqrt{(E_{X_{01}} - C_X)^2 + (H_X - E_{Y_{01}})^2} \cdot \sin\left(\frac{1}{2}\left(\operatorname{atan}\left(\frac{X_{21} - C_X}{H_X}\right) - \operatorname{atan}\left(\frac{X_{11} - C_X}{H_X}\right)\right)\right);$$

$$R_{Y_1} = \sqrt{(E_{Y_{01}} - C_Y)^2 + (H_Y - E_{X_{01}})^2} \cdot \sin\left(\frac{1}{2}\left(\operatorname{atan}\left(\frac{Y_{21} - C_Y}{H_Y}\right) - \operatorname{atan}\left(\frac{Y_{11} - C_Y}{H_Y}\right)\right)\right).$$

During the calibration process, the instrument memory stores 121 measurements of rising (points N_{x1} and N_{x2} in Fig. 5) and falling (points N_{y1} and N_{y2} in Fig. 5) edges of the workpiece shadow using the wire gauge. Calibration points are arranged in different areas of the measuring zone as shown in Fig. 6.

Afterwards, the optimization algorithm is implemented for each measurement. The optimization of geometrical parameters means minimizing deviations on X- and Y-axes between the calculated and reference values of the radius. So, the functional is formulated:

$$F = \sum_{i=1}^{n}((\mathrm{Rx_i} - \mathrm{R})(\mathrm{Rx_i} - \mathrm{R}) + (\mathrm{Ry_i} - \mathrm{R})(\mathrm{Ry_i} - \mathrm{R})),$$

where R is the reference radius;

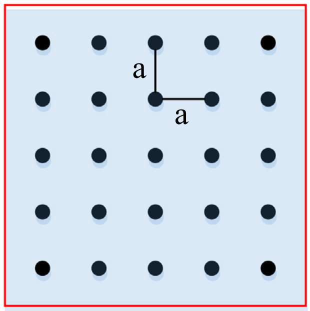

Fig. 6. Arrangement of experimental calibration points.

$$Rx_i = \sin\left(0,5\left(\arctan\left(\tfrac{X_{21i}-Cx}{Hx}\right) - \arctan\left(\tfrac{X_{11i}-Cx}{Hx}\right)\right)\right)\sqrt{(Ex_{01i}-Cx)^2 + (Hx - Ey_{01i})^2};$$
$$Ry_i = \sin\left(0,5\left(\arctan\left(\tfrac{Y_{21i}-Cy}{Hy}\right) - \arctan\left(\tfrac{Y_{11i}-Cy}{Hy}\right)\right)\right)\sqrt{(Ey_{01i}-Cy)^2 + (Hy - Ex_{01i})^2}.$$

The embedded MATLAB function is used to minimize the functional [24], to which the functional F and initial geometrical parameters are delivered.

2.3. Error correction algorithm for diameter characterization

The error correction algorithm implies the bias compensation between the measuring and reference diameters during the workpiece motion within the measuring zone. A series of the error estimations is carried out for wire gauges which cover the whole range of the gauge variables to implement this algorithm in accordance with Fig. 5. The obtained error surfaces are then triangulated, and the triangle with the workpiece centre in it is defined. The observational error is detected in the workpiece centre by means of constructing the plane which passes through all the three vertices of the triangle and assuming that the observational error lies in this plane.

The equation of a plane passing through the workpiece centre takes the form:

$$A \cdot x \; + \; B \cdot y \; + \; C \cdot z \; + \; D \; = 0$$

The coefficients of the plane equation areobtained assuming that the determinant of a matrix comprising the point location differences equals zero. After transformations, these coefficients can be written as

$$\begin{aligned}
A &= y_0 \times z_1 - y_1 \times z_0 - y_0 \times z_2 + y_2 \times z_0 + y_1 \times z_2 - y_2 \times z_1;\\
B &= -x_0 \times z_1 + x_0 \times z_2 - x_2 \times z_0 + x_1 \times z_0 - x_1 \times z_2 + x_2 \times z_1;\\
C &= x_0 \times y_1 + x_2 \times y_0 - x_1 \times y_0 - x_0 \times y_2 + x_1 \times y_2 - x_2 \times y_1;\\
D &= -x_0 \times y_1 \times z_2 + x_0 \times y_2 \times z_1 + x_1 \times y_0 \times z_2\\
&\quad -x_1 \times y_2 \times z_0 - x_2 \times y_0 \times z_1 + x_2 \times y_1 \times z_0,
\end{aligned}$$

where (x_0, y_0, z_0), (x_1, y_1, z_1), (x_2, y_2, z_2) are the points of observational errors; x, y are the workpiece coordinates; z is the observational error.

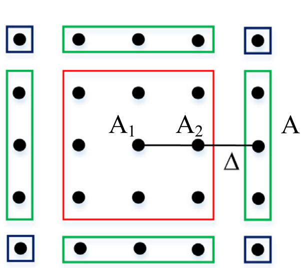

Fig. 7. Arrangement of additional calculated calibration points.

Since the aim of this study is to detect observational errors at specified points, we can derive the observational error z from the equation of a plane and calculate it using the specified values of x and y coordinates.

This method is used to estimate errors for the nearest larger and smaller reference diameters. The total observational error is estimated using the linear interpolation method.

Calibration readouts are obtained within the limited space, while the workpiece size may go beyond this space. Therefore, the limiting values should be extrapolated to ensure that they go beyond the point calibration. Calibration points arranged in the red region represent the gauge readouts. In order to calculate the calibration points arranged in the green region, the linear extrapolation method is applied (see Fig. 7).

The required point A is on the straight line passing through points A_1 and A_2 at a given distance Δ from A_2. Points A_1 and A_2 correspond to X_1, Y_1, Z_1 and X_2, Y_2, Z_2 coordinates, respectively, while the required point A corresponds to X, Y, and Z coordinates. Therefore, Y and Z coordinates can be found from

$$\frac{X_2 - X_1}{X_1 - X} = \frac{Y_2 - Y_1}{Y_1 - Y} = \frac{Z_2 - Z_1}{Z_1 - Z}$$

The X coordinate corresponds to X_2+ Δ coordinate. If X_1, X_2 or Y_1, Y_2 coordinates are equal, division by zero occurs, hence, the equation is reduced to a two-dimensional solution.

Calibration points arranged in blue regions are calculated through the point locations in the plane. The plane is specified by two points locating in the blue region and one angular point in the red region.

2.4. Flow charts of primary calibration and measurement process

Fig. 8 presents flow charts of proposed algorithms of the primary calibration and the conventional measurement process.

2.5. Calibration device and utility

The calibration device and utility have been developed for the implementation of proposed optimization algorithms. The calibration device illustrated in Fig. 9 comprises the optical system and the position control device. The latter represents a dual-axis machine which incorporates two PLLM-01 linear modules, two PLD441 drivers and a STM32-H103 debug board. The workpiece is clamped to the traveling carriage.

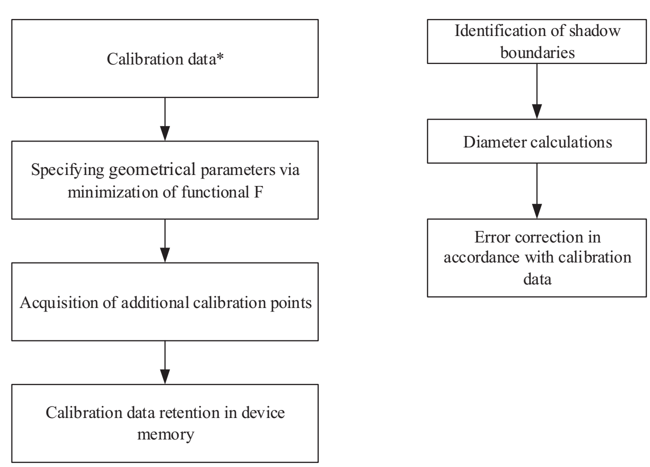

Fig. 8. Flow charts of first calibration and conventional diameter measurement. *Calibration was performed for nine reference gauges at 121 points. Measurements were repeated three times for each gauge.

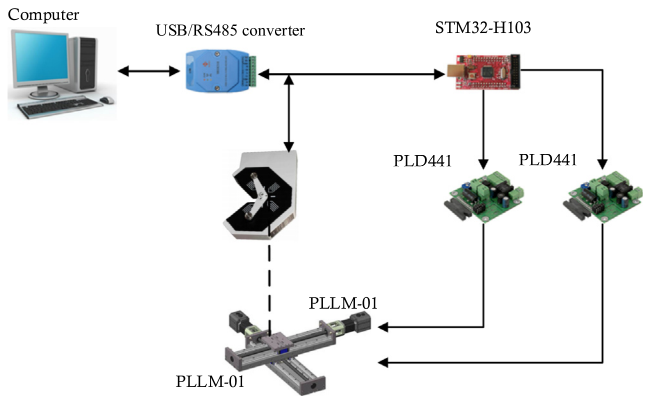

Fig. 9. General configuration of calibration device.

This calibration device is provided with the calibration utility developed in the Qt environment. The calibration utility allows a user to set coordinates in the position control device and receive gauge readouts which are then saved to the data file with rising and falling edges and errors for their further processing. The interface of the calibration utility is shown in Fig. 10.

A feedback-control mechanism is used for the position control. In order to reduce a 1 μm difference between the set and the current positions of the workpiece centre, it is moved along one of the axes. The proportional plus integral control law is used as a controller. The experimentally obtained proportional gain of 0.5 allows us to correctly set the workpiece coordinates in spite of the impossibility to achieve the accurate alignment between the mechanical and optical coordinate systems.

Therefore, the difference between the existing and upgraded devices is the use of Powell lenses in each channel (see Fig. 4) which create the uniform distribution of the luminous flux, without dramatic fluctuations and jumps (Fig. 11b). Other modifications concern the firmware upgrade to add the proposed optimization algorithms and error corrections within the measuring zone.

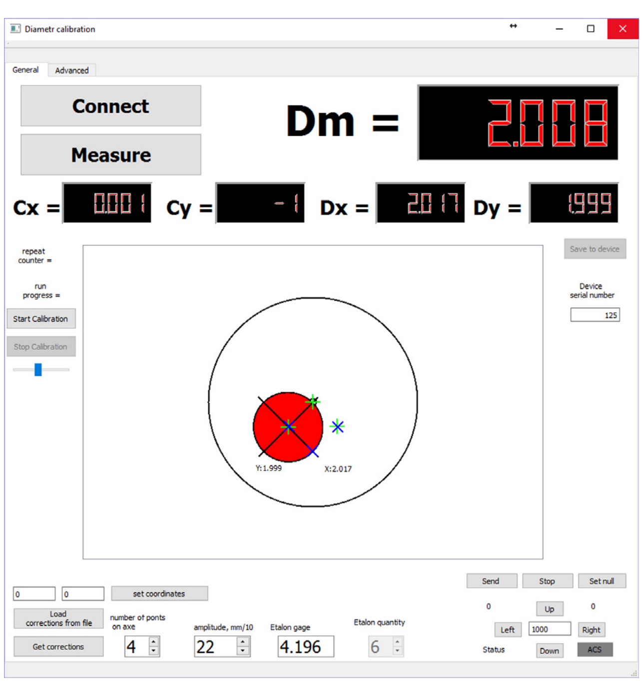

Fig. 10. Calibration utility developed in Qt environment.

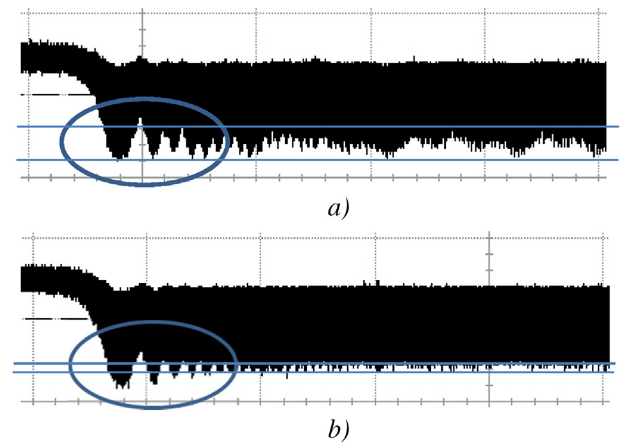

Fig. 11. Oscillograph recordings: *a* – laser diode without accessory optics; *b* – laser diode with collimator and Powell lens.

3. Results

Fig. 10 presents oscillograph recordings for two video signals, namely with and without accessory optics (see Fig. 2) such as a collimator and the Powell lens (see Fig. 4). As can be seen from Fig. 11a, the video signal contains non-uniformities which can achieve up to 20% of the useful signal amplitude and complicate the detection of the object boundaries by edge diffraction defects as described in [17]. The schematic orientation of the laser diode presented in Fig. 4, reduces the non-uniformity of the video signal (Fig. 11b). Consequently, we have a more reliable detection of minima and maxima of the interference pattern and a more uniform error region. According to Fig. 11, the non-uniform light field (the area between lines) without the use of the Powell lens (Fig. 2) and diffraction effects (the area inside the oval) which detect shadow boundary [17], is several times larger than that one obtained using the Powell lens (Fig. 4).

The error regions before and after the optimization of geometrical parameters are shown in Fig. 12. This figure shows how this optimization eliminates the constant error component.

Fig. 13 presents three-dimensional diagrams of the error regions before and after error corrections within the measuring zone. The difference in the diameter measurements is reduced to 0.2% throughout the measuring zone.

4. Discussion

The described laser gauge is provided with a protection shield against electromagnetic noise reflected by the metal casing. Circuitry and main boards are designed in strict adherence to the electromagnetic compatibility requirements. This gauge is also provided with additional vignettes to protect the system from the external stray light. These protections allow us to minimize both internal and external noise down to values comparable with the threshold sensitivity of the CCD sensors 3,6 V/(lx·s). Therefore, the noise error is small to negligible as compared to that of the non-uniform light field, which can often achieve one third of the amplitude of the valid signal as presented in Fig. 11b.

Since the luminous flux distribution within the measuring zone is constant independent of the spread in its values, the repeatability of measuring results is also constant at each point and equals 1 μm. It is the repeatability that allows utilizing the proposed error correction method in the measuring zone and achieving the results reproducibility of 3 μm during the lot production of laser diameter gauges.

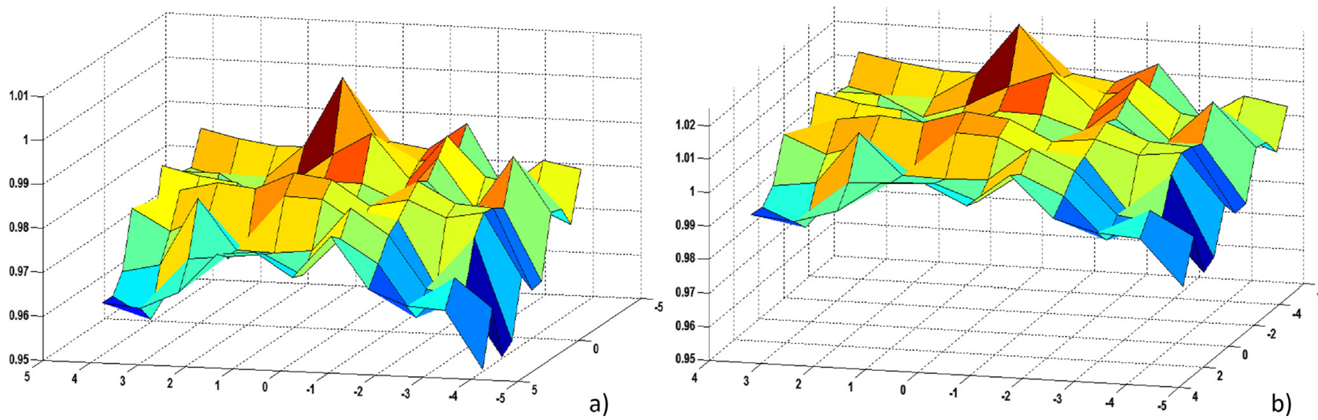

Fig. 12. Three-dimensional diagrams of the error region, %: *a* – before optimization; *b* – after optimization.

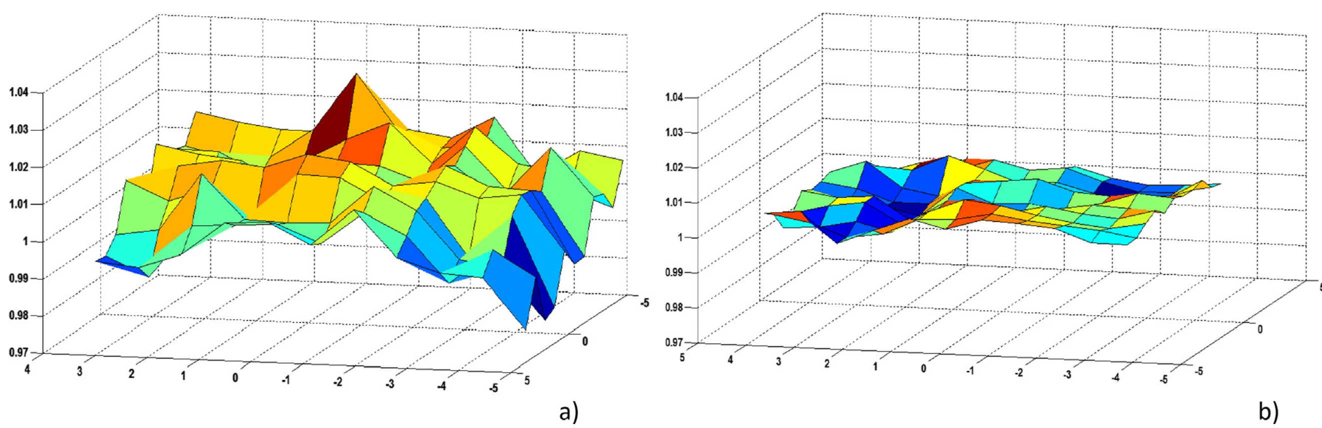

Fig. 13. Three-dimensional diagrams of error regions, %: *a* – before error correction; *b* – after error correction.

Table 1
A comparison of the original and modified measuring instruments.

Reference diameter, mm	Original gauge with one-point calibration. Measured diameter, mm (observation error, %)						Modified gauge with 121-point calibration. Measured diameter, mm (observation error, %)					
	Measuring zone centre		1/2 measuring zone radius		Measuring zone edge		Measuring zone centre		1/2 measuring zone radius		Measuring zone edge	
	meas.	err.	meas.	err.	meas.	err.	meas.	err.	meas.	err.	meas.	err.
1.212	1.214	−0.17	1.223	−0.93	1.190	1.84	1.213	−0.04	1.211	0.09	1.210	0.17
3.208	3.202	0.18	3.170	1.18	3.273	−2.02	3.207	0.04	3.205	0.10	3.214	−0.19
6.781	6.795	−0.21	6.855	−1.10	6.913	−1.94	6.784	−0.05	6.773	0.12	6.770	0.17
9.836	9.816	0.20	9.932	−0.97	10.062	−2.29	9.831	0.05	9.826	0.10	9.852	−0.16
12.341	12.320	0.17	12.487	−1.18	12.115	1.83	12.347	−0.05	12.355	−0.11	12.360	−0.15

As a result of the experiments, several workpieces were used to compare the similar gauges being calibrated with and without accessory optics and with and without the use of proposed optimization algorithms. Eleven measurements were carried out for each gauge at various points of the measuring zone. The obtained values were averaged. For visual representation of this comparison, see the Table 1 below.

As follows from the data shown in the Table 1, the two instruments demonstrate approximately the same calibration accuracy in the centre of the measuring zone. However, the required 0.2% measurement accuracy is achieved only by the modified gauge when moving the workpiece within the measuring zone. Subsequent measurement errors are mostly determined by the cell discreteness in the CCD module and non-linear distortions in the optical system.

5. Conclusion

Before the implementation of proposed methods, the gauge calibration was provided only in the centre of the measuring zone. Such an approach does not ensure the measurement accuracy in all possible situations. The implementation of proposed methods considerably improved the video quality and provided the desired measurement precision throughout the measuring zone, thereby raising the competitive capacity of gauge. The proposed optimization algorithms can be used in a wide range of measuring devices.

Unlike gauges providing the error normalization in the vicinity of the centre of the measuring zone, which amounts to 10–15% of its actual size depending on the model, the suggested calibration method ensures the efficient error normalization within the entire measuring zone, without prejudice to final calibration. Using the

Powell lens (which considerably improved the laser intensity wavefront) in conjunction with the error correction method provided the video quality improvement during the cable movement.

The proposed method makes the gauge design more expensive and increases time of calibration that can be regarded as its downsides. However, the improvement of metrological characteristics by more than 1.5% certainly provides a positive effect. The proposed technology was successfully used in the lot production of LDM-50 devices [25] manufactured by LTD Redwill, Tomsk, Russia.

Acknowledgments

The reported study was supported by the Ministry of Education and Science of the Russian Federation (project #2.3649.2017/4.6). The authors gratefully acknowledge the great assistance of Ya. Kondrashev from Tomsk Polytechnic University and translation by M. Vorob'eva from Tomsk State University of Architecture and Building http://www.tsuab.ru/en/.

References

[1] Xiaodong Hua Yang Lub, Measurement error analysis of a twin-cantilever sensor for measuring external diameter, Measurement 77 (2016) 373–387.
[2] Bin Li, Measurement Polygon-based large diameter measurement with modular gauges, Measurement 27 (1) (2000) 1–11.
[3] J. Liu, C. Cetinkaya, Mechanical and geometric property characterization of dry-coated tablets with contact ultrasonic techniques, Int. J. Pharm. 392 (1–2) (2010) 148–155.
[4] R. Chen, W. Guo, J. Jin, Online eccentricity monitoring of seamless tubes in cross-roll piercing mill, ASME 2014 International Manufacturing Science and Engineering Conference, MSEC 2014 Collocated with the JSME 2014 International Conference on Materials and Processing and the 42nd North American Manufacturing Research Conference, 2014.
[5] Xuanyin Wanga, Senwei Xianga, Ke Xianga, Feng Panb, Measurement A novel method for diameter measurement of silicon single crystal, Measurement 121 (June 2018) 286–293.
[6] Vítor Carvalho, Michael Belsley, Rosa M. Vasconcelosc, Filomena O. Soares, Measurement Yarn hairiness and diameter characterization using a CMOS line array, Measurement 41 (10) (2008) 1077–1092.
[7] A. Podmaniczky, M. Barabàs, A. Màrkus, Measurement micro-interferometric method for relative diameter measurement of optical fibres, Measurement 5 (3) (1987) 135–140.
[8] B. Mühlheim, Zumbach has developed innovative on-line measurement, monitoring and control equipment since 1957, MPT Metallurgical Plant Technol. Int. (2) (2017) 44–49.
[9] W. Advanced Blohm, on-line measuring and analysis techniques for an economical cable production, Proc. Intl. IWMA Conf. Econ. Process. Rod Wire Cable (1999) 67–75.
[10] Fleming, P., Coleman, L., Capacitance monitoring systems (2003) US Patent 20030128038.
[11] Method for Spark Testing of Cables (2002) British standard BS EN 50356.
[12] Electric Cables – Spark Test Method IEC 62230 2006.
[13] Fedorov E. M., Gol'dshtein A. E., Dvukhkoordinatnyi lazernyi izmeritel' diametra kabelya na osnove opticheskogo difraktsionnogo metoda [Two-coordinate laser diameter measuring instrument based on optical diffraction method]. Polzunovskii Vestnik 2015;1: 86–91. (rus)
[14] Y. Chugui, V. Bazin, L. Finogenov, S. Makarov, A. Verkhogliad, Optical electronic measuring systems and laser technologies for scientific and industrial applications, Proceedings of the international symposium on instrumentation and control technology no 6, Beijing, China, 2006, 6357 (2) [Note(s): 2 vol.] (13 ref.) isbn:0-8194-6452-x; 978-0-8194-6452-1.
[15] Zhifeng Zhanga, Chao Lub, Fangzhen Zhangc, Yufen Rena, Kun Yanga, Zhan SudA, Novel method for non-contact measuring diameter parameters of wheelset based on wavelet analysis, Optik – Int. J. Light Electron. Opt. 123 (5) (2012) 433–438.
[16] Qiucheng Suna, Yueqian Houb, Qingchang Tanc, Chunjing LiShaft Diameter measurement using a digital image, Opt. Lasers Eng. 55 (April 2014) 183–188.
[17] Y.A. Chursin, E.M. Fedorov, Methods of resolution enhancement of laser diameter measuring instruments, Opt. Laser Technol. 67 (2015) 86–92.
[18] E.M. Fedorov, A.A. Koba, Diameter calculation in contactless three-axis measuring devices, MATEC Web Conf. 79 (2016), Article number 01082.
[19] E.M. Fedorov, YuA. Chursin, V.V. Red'ko, Dvukhkoordinatnyi lazernyi izmeritel' diametra LDM-18 [Two-coordinate laser diameter measuring instrument LDM-18], Kontrol'. Diagnostika. 11 (2014) 25–29.
[20] C.-Y. Wang, Q.-C. Tan, R.-H. Guo, Design and optimization of a linear laser beam, Lasers Eng. (Old City Publishing). 27 (5/6) (2014) 373–381.
[21] M. Leotta, A. Vandergon, G. Taubin, 3D slit scanning with planar constraints, Comput. Graph. Forum 27 (8) (2008), 2066-2008.
[22] Hans-Gerd Maas, Bernd Hentschel, Frank Schreiber, Optical triangulation method for height measurements on water surfaces, Proc. SPIE 5013, Videometrics VII, 103 (January 20, 2003); doi:10.1117/12.473088.
[23] Michael B. Sinclair, Jerilyn A. Timlin, David M. Haaland, Margaret Werner-Washburne, Design, construction, characterization and application of a hyperspectral microarray scanner, Appl. Opt. 43 (10) (2004) 1.
[24] Mathworks functions documentation www.mathworks.com/help/optim/ug/fmincon.html?requestedDomain=www.mathworks.com, 2018 (accessed 17.06.18)
[25] Redwill official page http://redwill.ru/Izmeriteli-diametra, 2018 (accessed 17.06.18)